polymers

MDPI

Article

$CaCO_3$ Polymorphs Used as Additives in Filament Production for 3D Printing

Lucie Zárybnická [1,2], Radek Ševčík [1,3,*], Jaroslav Pokorný [3], Dita Machová [1], Eliška Stránská [4] and Jiří Šál [3]

[1] Institute of Theoretical and Applied Mechanics of the Czech Academy of Sciences, Prosecká 809/76, 190 00 Praha, Czech Republic; zarybnicka@itam.cas.cz (L.Z.); machova@itam.cas.cz (D.M.)
[2] Department of Technical Studies, College of Polytechnics Jihlava, Tolstého 16, 586 01 Jihlava, Czech Republic
[3] Department of Civil Engineering, Faculty of Technology, Institute of Technology and Business, Okružní 517/10, 370 01 Českе Budejovice, Czech Republic; jaroslav.pokorny@mail.vstecb.cz (J.P.); sal@mail.vstecb.cz (J.Š.)
[4] MemBrain s.r.o., Pod Vinicí 87, 471 27 Stráž pod Ralskem, Czech Republic; eliskastr@seznam.cz
* Correspondence: sevcik@itam.cas.cz; Tel.: +420-567-225-322

Abstract: Nowadays, additive manufacturing—also called 3D printing—represents a well-established technology in the field of the processing of various types of materials manufacturing products used in many industrial sectors. The most common type of 3D printing uses the fused filament fabrication (FFF) method, in which materials based on thermoplastics or elastomers are processed into filaments. Much effort was dedicated to improving the properties and processing of such printed filaments, and various types of inorganic and organic additives have been found to play a beneficial role. One of them, calcium carbonate ($CaCO_3$), is standardly used as filler for the processing of polymeric materials. However, it is well-known from its different applications that $CaCO_3$ crystals may represent particles of different morphologies and shapes that may have a crucial impact on the final properties of the resulting products. For this reason, three different synthetic polymorphs of $CaCO_3$ (aragonite, calcite, and vaterite) and commercially available calcite powders were applied as fillers for the fabrication of polymeric filaments. Analysis of obtained data from different testing techniques has shown significant influence of filament properties depending on the type of applied $CaCO_3$ polymorph. Aragonite particles showed a beneficial impact on the mechanical properties of produced filaments. The obtained results may help to fabricate products with enhanced properties using 3D printing FFF technology.

Keywords: 3D printing; FFF; filament; polypropylene; additives; $CaCO_3$ polymorphs; mechanical properties

Citation: Zárybnická, L.; Ševčík, R.; Pokorný, J.; Machová, D.; Stránská, E.; Šál, J. $CaCO_3$ Polymorphs Used as Additives in Filament Production for 3D Printing. *Polymers* **2022**, *14*, 199. https://doi.org/10.3390/polym14010199

Academic Editors: Roland Kuen Ren Chen and Yancheng Wang

Received: 26 November 2021
Accepted: 31 December 2021
Published: 4 January 2022

1. Introduction

The use of three-dimensional (3D) printing is nowadays frequently applied technology in various industry sectors, including civil engineering, biotechnology, and automotive [1–9]. Several additive technology techniques were developed and are widely used, such as stereolithography (SLA), fused filament fabrication (FFF), poly-jet, selective laser melting (SLM), selective laser sintering (SLS), direct metal laser sintering (DMLS), and laminated object manufacturing (LOM). The selection of a particular technique is essential to design products of required parameters at the desired cost of materials—the most frequently used additive technologies can be sorted according to their ascendant financial requirements as follows LOM < FFF < SLA < SLS < DMLS/SLM [10].

FFF is one of the most often used additive technology due to its low energy consumption and possibilities of printing products with complex shapes [11]. It belongs to so-called bottom-up methods that are producing one layer at a time, and the final 3D structured products are fabricated by gradual accumulations of these 2D layers [12]. Further description of FFF technology may be found e.g., in [13,14] and references therein. Polylactic acid (PLA) [15–19], acrylonitrile butadiene styrene (ABS) [20–24], polyethylene terephthalate (PET) [25], polyethylene terephthalate glycol (PET-G) [26–28], polypropylene (PP) [29,30],

and viscoelastic thermoplastic elastomers like thermoplastic polyurethane (TPU) [31,32] belong to the most common thermoplastics applied in FFF technology.

The properties of filaments may be modified by the usage of different additives based on the character of the polymeric material. Among the most widely used additives affecting the life of the polymeric material are light stabilizers (like UV absorbers, photooxidation inhibitors), antioxidants, flame retardants, or thermal stabilizers. The second group is additives affecting polymeric properties, such are antistatic, lubricants, fillers, pigments, and blowing agents [33–39].

As another suitable additive, calcium carbonate ($CaCO_3$) can be considered. $CaCO_3$ may form three anhydrous crystalline polymorphs—thermodynamically most stable calcite, and metastable vaterite and aragonite. It may be present also in hydrated crystal forms (ikaite ($CaCO_3 \cdot 6H_2O$), monohydrate ($CaCO_3 \cdot H_2O$), hemihydrate ($CaCO_3 \cdot \frac{1}{2}H_2O$), and as an amorphous phase (amorphous calcium carbonate (ACC)) [40]. $CaCO_3$ polymorph exhibits particles with different morphology and properties like physical–mechanical performance [41]. In general, it was shown in [42] that different particle's morphologies affected tensile strength of powders. Furthermore, $CaCO_3$ is frequently used as a filler [43] because of its unique properties such as low toxicity, biological inertness, good dispersion within the polymer matrix, and low moisture content [44,45].

In the case of polymers in which $CaCO_3$ is used, for example, as a filler in polyvinyl chloride (PVC), these reach increased rigidity and flexibility. Due to its white color, it can be used as a pigment, which is comparable to TiO_2, but it is cheaper [46]. $CaCO_3$ also provides high brightness and gloss and can thus replace lead-based stabilizers with a calcium/zinc system. In polypropylene, the application of $CaCO_3$ (usually around 10 wt %) increases stiffness and resistance to weathering [47]. It is also used as a filler in unsaturated polyesters for the preparation of non-shrinkable structures [48,49]. Calcium carbonate belongs to the class of isomeric filler—the usage of smaller particles results in better adhesion to the matrix. Particles with a higher specific surface area have been identified to have a beneficial effect on the modulus of elasticity [50].

This work aimed to investigate the effect of different crystalline anhydrous polymorphs of $CaCO_3$—namely, aragonite, calcite, and vaterite—exhibiting different properties, such as morphology, on the fabrication of filaments composed of random polypropylene copolymer using the FFF technique. The aim is to get the insight of their effect on physical-mechanical properties of resulted filaments which may find application in 3D printing.

2. Experimental Part

2.1. Materials

Polypropylene random copolymer (PPR) product Lumicene MR60MC2 (Total Petro-Chemicals & Refining S.A./N.V., Bruxelles, Belgium) in the shape of pellets was used as received. Calcite and vaterite were synthesized pure ($\geq$99 wt %) using the mixing of two concentrated salt solutions, as further described in [51]. Aragonite was synthesized with a minor amount of calcite ($\leq$4.7 wt %) following the procedure described in [52]. The quantitative phase analysis of X-ray diffraction patterns using Rietveld refinement confirming the purity of synthetized $CaCO_3$ polymorphs was reported in [41]. To compare the synthesized product with commercially available one, also calcite available on the market (min. 95%, Lach-Ner, Ltd., Neratovice, Czech Republic) was used for filament fabrication.

2.2. Filaments Preparation

The mixed granulates of PPR Lumicene MR60MC2 with 5 wt % of the $CaCO_3$ polymorphs were carried out on an extruder (HAAKE PolyLab OS Rheo Drive 16, Thermo-Scientific, Waltham, MA, USA) with a PTW 24/28 twin screw (cumulatively maintained at 2.5 $kg \cdot h^{-1}$, 60 rpm extruder, temperature profile 180–160 °C). Then, granulates were processed in a hydraulic press (ZHOT, Presshydraulika, Opava, Czech Republic) and divided using 2 × 13 g extrudate, 160 °C, 15 min heating only, and 10 min heating and pressing at 50 bar and cooling to 60 °C. This process is referred in the next text as a first thermal treatment.

Subsequently, a mini extruder (Wellzoom Desktop Extruder Line, Shenzhen, China) was used for the preparation of filaments from granulates using constant speed 10 cm·min^{-1}, at two temperature zones 175 and 185 °C and air cooling. The average diameter of produced filaments was (1.75 ± 0.05) mm-typical filament dimensions processed by FFF technology. This process is referred in the next text as a second thermal treatment.

The used abbreviations of produced filaments are as follow: filament without additive–F_Ref, filament composed of PPR and synthetic aragonite–F_Ara_s, filament composed of PPR and synthetic calcite–F_Cal_s, filament composed of PPR and synthetic vaterite–F_Vat_s, filament composed of PPR and commercially available calcite–F_Cal_c. In the case of granulates, the abbreviations contain the letter G at the beginning instead of the letter F used for filaments.

2.3. Methods

Particle size distribution of used additives was recorded using laser granulometer LD 1090 (Cilas, Orléans, France). The measurements were performed in isopropyl alcohol, and each material was tested at least three times. BET specific surface area was measured using the device ASAP 2020 (Micromeritics, Norcross, GA, USA). The skeletal densities of the produced granulates and filaments were determined with a helium pycnometer AccuPyc II 1340 (Micromeritics, Lincoln, UK) using maximum pressure of 19.5 Psi and 10 cycles. The relative standard deviation of six replicates was calculated to be ≤0.05%. Viscoelastic properties of both granulates and filaments were characterized by a melt flow index (MFI) using extrusion plastometer M-201 (Chemoprojekt Praha, Czech Republic). The procedure, described in the ČSN EN ISO 1133 [53], was followed using these parameters of measurements: preheating load 240 s, test condition–t = 190 °C, load 2.16 kg, measuring length 10 mm, step length 0.25 mm, measurement starting time 300 s, die-diameter 2.095 mm, and length 8.00 mm. Produced filaments were characterized in terms of surface quality and surface roughness (S_a–arithmetical mean roughness value and S_z–mean roughness depth) using a Keyence VHX-6000 optical microscope (Keyence, Itasca, IL, USA) according to the standard ISO 25178 [54]. A caliper was used to measure filament diameters.

The tensile properties of the prepared filaments were determined using Instron 3345 (Instron, Norwood, MA, USA) with a maximum load of 5 kN and a constant load speed of 5 mm·min^{-1} following the standard CSN EN ISO 527-1 [55]. At least five replicates of each sample were tested.

Optical images of produced filaments were collected using an optical microscope Olympus TH4-200 (Olympus, Šindžuku, Japan). The morphology of used $CaCO_3$ polymorphs and structural arrangements of produced filament was observed under a field emission scanning electron microscope (SEM) Quanta 450 FEG (FEI, Brno, Czech Republic) using a secondary electron detector. Observations were conducted at the 20 kV accelerating voltage. Powdered $CaCO_3$ polymorphs were dispersed on carbon tape, as well as fragments of filament samples. Then, samples placed on stubs were coated with a 5-nm-thick layer of gold using a sputtering machine (Quorum Q150R ES, Quorum Technologies, Lewes, UK).

3. Results and Discussion

3.1. Characterization of Used $CaCO_3$ Polymorphs

In Figure 1, morphologies of used $CaCO_3$ polymorphs observed under SEM are depicted. Synthetic aragonite formed needle-like crystals usually connected as larger clusters up to tens of μm (Figure 1a). Together with aragonite crystals, rhombohedral crystals of calcite were identified in smaller quantities. Synthetized calcite crystals were found to be present with typical euhedral to subhedral crystal habit. Larger calcite aggregates were composed mainly with the crystal of the size in the range from 1–3 μm and sporadically with crystal smaller than 0.5 μm (Figure 1b). Commercial calcite exhibited small and irregularly shaped crystals as a consequence of the grounding of raw limestone. The sizes of such particles varied from tens of nanometers to a few micrometers, usually with one elongated crystal site. As visible in Figure 1c, particles are tempted to be present in large

aggregates up to several microns. Spherulitic crystals with a radius from 0.5–3.5 μm of synthetic vaterite built up from nanometric spherules (detail image reported in [56]) were detected (Figure 1d). In agreement with other $CaCO_3$ particles, also vaterite crystals were observed to form larger (up to 10 μm) aggregates.

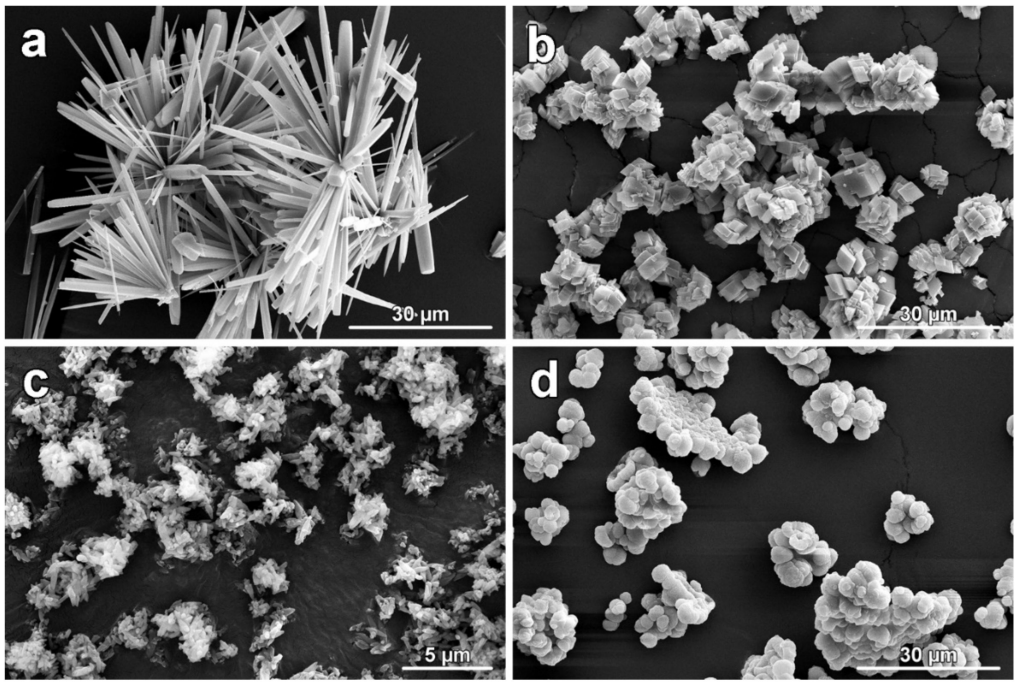

Figure 1. Collection of observed morphologies of synthesized $CaCO_3$ polymorphs (aragonite (**a**), calcite (**b**), commercially available calcite (**c**), and vaterite (**d**)) observed under SEM.

The particle size distribution detected in isopropanol suspensions is shown in Figure 2. As expected, the high difference in their shapes was recorded. Aragonite represents PSD with the largest particles of trimodal distribution with local maxima at 4, 20, and 85 μm. Bimodal distributions were found for the synthetic and commercial calcite with the local maxima at 1 and 10 μm and at 0.3 and 3 μm, respectively. In the case of synthetic vaterite, bimodal distribution with local maxima at 0.3 and 9 μm were recorded. It was illustrated by numerous investigations that morphology and particle size of $CaCO_3$ have very high variability depending on the used reaction conditions and involvement of other chemicals [57]. Additionally, as mentioned in the Introduction, $CaCO_3$ polymorphs show systems with tremendously different properties—e.g., hardness and reduced modulus. For example, reduced modulus of synthetized products (using the same reaction conditions as in this paper) was detected to be 5(4), 16(7), and 31(8) GPa calculated for aragonite, calcite, and vaterite, respectively [41]. The crystal morphologies of applied $CaCO_3$ polymorphs, of course, also impacted the values of specific surfaces of their powders. The synthetic $CaCO_3$ displayed values of 5.58 ± 0.02, 1.96 ± 0.01, and 2.34 ± 0.02 $m^2 \cdot g^{-1}$ for aragonite, calcite, and vaterite, respectively [41]. In the case of commercial calcite, the highest specific surface area of 6.73 ± 0.02 $m^2 \cdot g^{-1}$ was measured. The usage of additives with higher specific surface area values may result in their increased agglomeration within the polymer matrix. In the case of PP, the critical value of additives in polypropylene composite was identified to be 7 $m^2 \cdot g^{-1}$ [58], and it was shown that increased aggregations caused a significant decrease of strength and impact resistance.

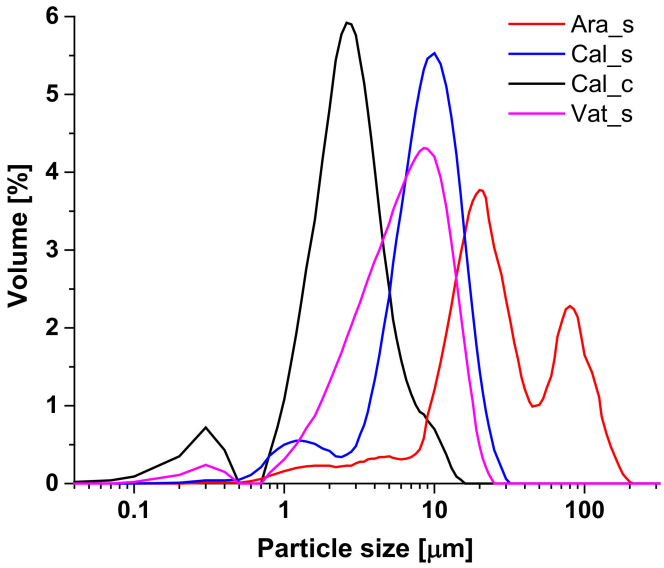

Figure 2. Comparison of recorded particle size distributions of $CaCO_3$ polymorphs used as additives for filament production.

3.2. Characterization of Prepared Granulates

The progress of torque force (M [Nm]) and head pressure (p [bar]) during the extrudation of granulates is depicted in Figure 3. Constant values of torque over time (between 40–45 Nm) were recorded together with a slight decrease of the head pressure that oscillated between 7–10 bar after 10 min was reached. The G_Cal_c sample showed higher pressure values at the beginning of the processing in comparison with other samples. Such phenomena could be ascribed to the high specific surface area of applied commercial calcite particles, which may have had an increased tendency to partial agglomeration, nonetheless, after 11 min, pressure values started to be identical with the other samples. Thus, it can be assumed that suitable production conditions were achieved, and the Lumicene MR60MC2 PPR doped with the produced $CaCO_3$ particles was successfully processed during extrusion.

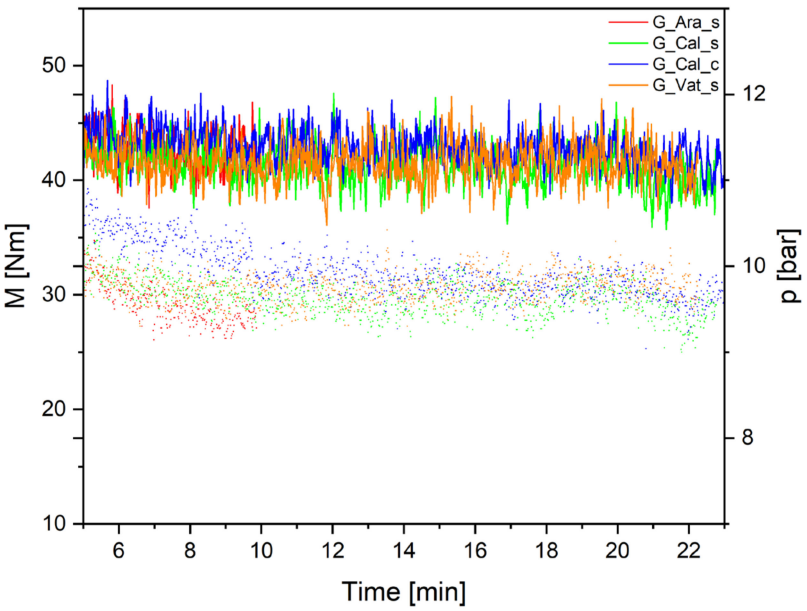

Figure 3. Dependence of torque M (full line) and head pressure p (dotted line) over time during granulate extrusion.

The melt flow index (MFI) [59], reported in Table 1, represents a simple method for the characterization of rheological properties that play a crucial role in respect to the correct settings of the processing processes [60]. The lowest value was recorded for G_Ara_s, and others granulate showed comparable MFI values. Due to the fact that thermal degradation of $CaCO_3$ occurs above ~600 °C [61], $CaCO_3$ particles can retain the MFI value of PP and may improve the plasticity and processability of the polymers [62,63]. These properties are connected with the density of produced granulates. It can be seen in Table 1 that the addition of the $CaCO_3$ particles resulted in the increase of density of around 4%, compared to the reference state.

Table 1. Overview of determined physical properties of produced granulates (calculated standard deviations are reported in the brackets).

Sample	MFI ($g \cdot 10\ min^{-1}$)	Density ($g \cdot cm^{-3}$)
G_Ref	27.0(1)	0.8962(3)
G_Ara_s	24.0(2)	0.9330(4)
G_Cal_s	25.7(6)	0.9362(6)
G_Cal_c	26.0(6)	0.9368(4)
G_Vat_s	26.1(2)	0.9312(5)

3.3. Characterization of Prepared Filaments

The quality of the prepared filaments is very important for processing filaments using FFF technologies for 3D printing and has a major influence on trouble-free 3D printing, minimizing filament jams during winding, etc. Figure 4 shows the optical images of all prepared filaments. The F_Ref sample was produced as a transparent filament with a smooth surface without unevenness (Figure 4a). The additions of $CaCO_3$ powders resulted in a whitish appearance (Figure 4b–e). The application of commercial calcite and synthetic vaterite resulted in products with comparable structures (Figure 4d,e). Only minor inequalities have been detected within the structure of filaments containing aragonite. The worst product quality was achieved in the case of the application of synthetic calcite. Such filaments showed an uneven thickness, which could have a negative effect during processing, and filament jams might be occurred during 3D printing in the extruder. Such behavior could be ascribed to physical incompatibility of Cal_s with some compounds presented in used PP random copolymer (Lumicene MR60MC as reported in Experimental Section). The diameter of REF sample was measured to be 1.60 ± 0.05 mm. The diameters of filaments containing additives were detected to be higher: 1.75 ± 0.05 mm for F_Ara_s, F_Cal_c, and F_Vat_s samples and 1.70 ± 0.10 mm in case of sample F_Cal_s.

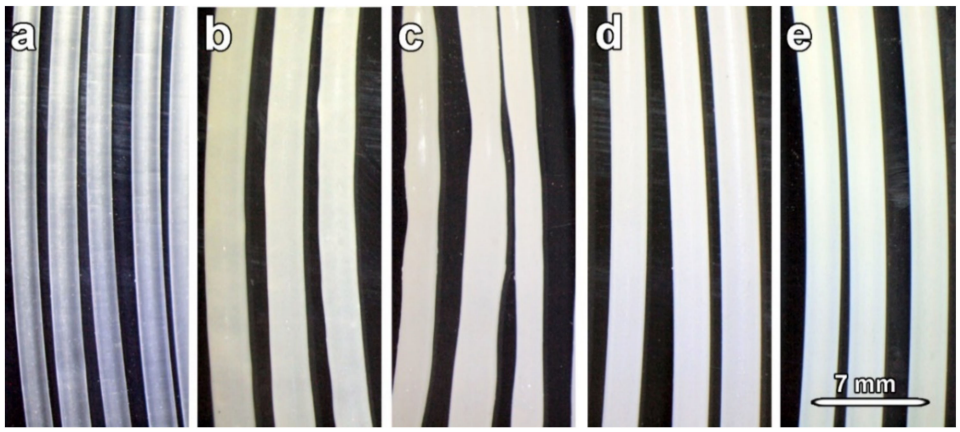

Figure 4. Photographic images of the prepared filaments: (**a**)—F_Ref, (**b**)—F_Ara_s, (**c**)—F_Cal_s, (**d**)—F_Cal_c, (**e**)—F_Vat_s.

The collection of SEM images of the internal fragments of produced filaments of $CaCO_3$ is shown in Figure 5. $CaCO_3$ particles were found to be well dispersed within the PP matrix, especially in the case of filament contained with aragonite (Figure 5e), the needle-like particles are equally distributed in the same orientation, and it can be noted that during filament processing, the large clusters were disintegrated into much smaller objects. Unlike the others, filaments contained with synthetic calcite showed a rougher internal structure with the presence of larger structural disintegration areas up to a few hundred microns. Such observation may partially explain the worst quality of produced F_Cal_s filaments. Images collected at higher magnifications (Figure 5d,f,h,j), on the one hand, confirmed the disintegration of larger clusters of $CaCO_3$ particles. On the other hand, the crystal's habit of applied $CaCO_3$ polymorphs (see Figure 1) during the filaments fabrication stayed preserved, even if it is visible (Figure 5d) that some of the aragonite's needle-like crystals showed deformations. This behavior is the line with previous results [41] in which aragonite's crystals were identified to be the most affected by thermal as well as pressure treatments. From the point of view of processing using FFF technology, the surface roughness of the prepared filaments is an important parameter. If high roughness values are reached, the filament becomes poorly processed, with a negative impact on winding. Thus, final products of inappropriate quality may be produced. As expected, different morphologies of applied $CaCO_3$ polymorphs influenced the roughness values. The highest roughnesses, both R_a and R_z, were detected in the case of filaments containing aragonite. Interestingly, filaments F_Cal_s, F_Cal_c, and F_Vat_s showed a lower roughness of R_a and R_z compared to the reference (Table 2). After the second thermal treatment during filament preparation, the MFI values—reported in Table 2—were found to be lower in comparison with the first thermal treatment used during the production of granulates (see Table 1), probably as a consequence of the further development of PP cross-linked structure [64]. Filaments containing $CaCO_3$ particles with the highest specific surface area, commercial calcite, and synthetic aragonite showed almost similar MFI properties, and in comparison with the reference, MFI values were found to be lower for ca. 16%. It was observed [65] that the addition of lower content of $CaCO_3$ with a smaller particle size tends to decrease the composite viscosity, which is related to the results of the MFI. The density of produced filaments containing $CaCO_3$ particles was found to be slightly lower in comparison with values detected for granulates as a consequence of the development of structural cross-linking [64].

Table 2. Overview of determined physical properties of produced granulates (calculated standard deviations are reported in the brackets).

Sample	MFI (g·10 min^{-1})	R_a (µm)	R_z (µm)	Density (g·cm^{-3})
F_Ref	22.7(2)	7.8(5)	42(1)	0.8979(8)
F_Ara_s	19.0(1)	11.0(1)	55(1)	0.9291(7)
F_Cal_s	23.9(1)	5.7(5)	28(1)	0.9290(1)
F_Cal_c	20.0(1)	4.8(4)	28(1)	0.9320(6)
F_Vat_s	25.1(4)	5.7(8)	38(1)	0.9285(4)

The results of the mechanical performance of produced filaments are summarized in Table 3. Obtained values of tensile stresses differs according to the presence of specific $CaCO_3$ particles. It was shown in [66] that different morphologies of $CaCO_3$ affected tensile strengths of tested powders. It can be noted that filaments produced with $CaCO_3$ particles showed, in most cases, a reduction of mechanical properties. The only exception is filament fabricated with aragonite. In this case, the mechanical properties were found to be improved—e.g., tensile stress was approx. 12% higher. The explanation may be found in the crystal habit of aragonite particles. Aragonite's needle-like particles that were observed to be homogenously and unidirectionally orientated within the PP matrix (Figure 5c,d) may act as reinforced material that positively affected mechanical performance. Reinforced materials are commonly used to enhance mechanical properties of, e.g., concretes [67,68].

From the rest of the three applied types of $CaCO_3$ particles, the filaments F_Cal_c and F_Vat_s showed comparable properties, and with respect to F_Ref, the only small decrease was recorded. However, in the case of F_Cal_s, a huge drop in mechanical performance was recorded (more than 50% in the comparison of tensile stress and Young modulus of F_Ref). It is not unexpected due to the bad quality of produced filament F_Cal_c (see Figure 4c) with tapering segments that have a strong impact on tensile stress. Comparison with the literature is difficult due to the lack of data focus on the products needed for 3D printing. In different systems, $CaCO_3$ particles have been used for the PP surface modifications [69,70], and the role of $CaCO_3$ on the crystallization of PP was investigated [71]. The usage of nanocalcite with a particle size of 70 nm showed an improving effect on Young's modulus, tensile yield stress, and impact strength [72,73]. Aragonite was recognized to have a more beneficial effect than calcite as filler in polyvinyl chloride or polypropylene [74].

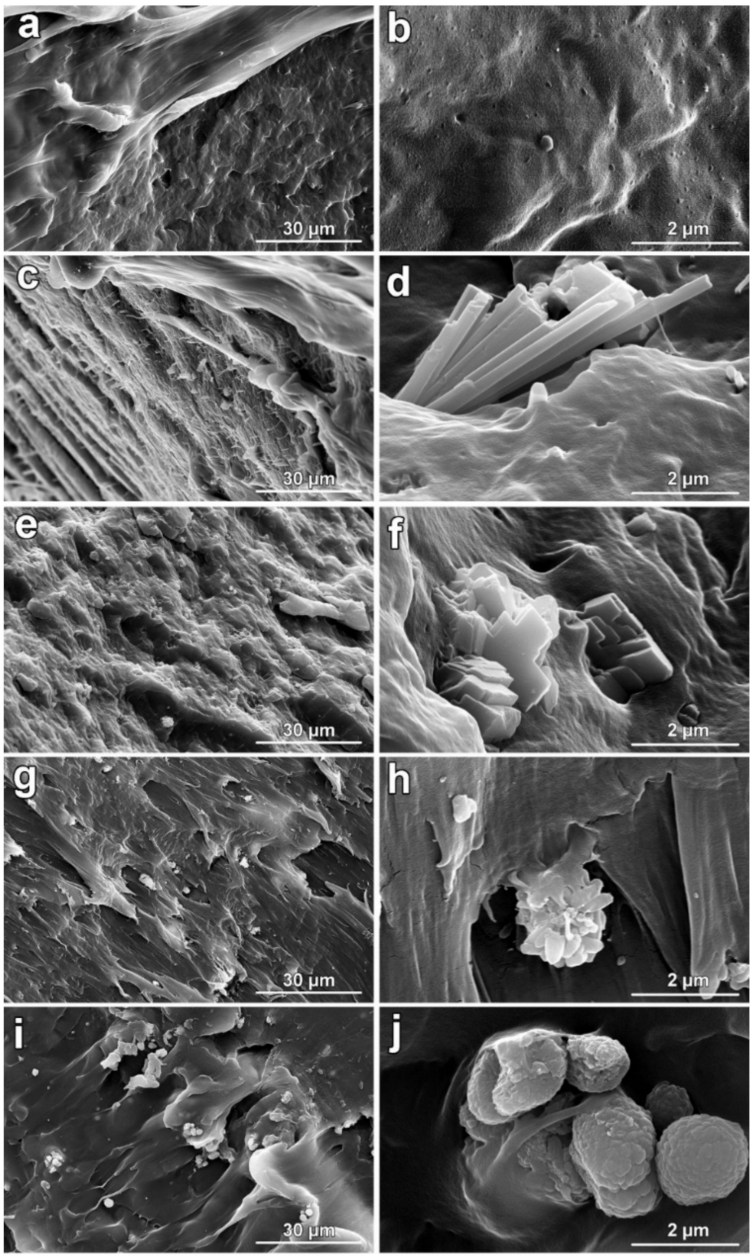

Figure 5. Collection of SEM images of prepared filaments collected at lower (**left**) and higher magnifications (**right**): (**a**,**b**)—F_Ref; (**c**,**d**)—F_Ara_s; (**e**,**f**)—F_Cal_s; (**g**,**h**)—F_Cal_c; (**i**,**j**)—F_Vat_s.

Table 3. Summarization of determined mechanical properties of prepared filaments.

Sample	Max. Load (N)	Tensile Stress (MPa)	Young Modulus (MPa)	Tensile Deformation (%)
F_Ref	34.6 ± 4.4	24.5 ± 1.7	1187.1 ± 73.2	4.5 ± 0.7
F_Ara_s	38.3 ± 3.7	27.4 ± 2.0	1074.1 ± 70.8	4.8 ± 0.5
F_Cal_s	19.0 ± 2.7	11.3 ± 3.5	459.6 ± 73.3	3.5 ± 0.7
F_Cal_c	32.5 ± 3.9	20.9 ± 1.8	765.2 ± 67.0	5.4 ± 0.4
F_Vat_s	29.8 ± 3.4	21.5 ± 1.1	811.8 ± 118.8	5.1 ± 0.8

4. Conclusions

The presented study has shown the possibilities of the application of $CaCO_3$ particles for the fabrication of polypropylene filaments employed for 3D printing. Moreover, the effect of the usage of different anhydrous crystalline $CaCO_3$ polymorphs on the physical-mechanical properties of produced granulates and filaments containing additives has been investigated employing the combination techniques. Microscopic observations showed tremendously different crystal habits of applied $CaCO_3$ particles that resulted in specific particle size distributions and specific surface areas. PP granulates with additions of $CaCO_3$ have been processed without significant differences and produced granulates showed approximately 4% higher densities compared to the reference sample. Next, heat treatment, production of filaments caused a decrease of MFI and density values as a consequence of more connected cross-linked structures. In the case of filaments produced with the addition of synthetic calcite, the resulting filaments showed crooked structure in contrast with other samples. Microscopic observations showed a homogenous distribution of $CaCO_3$ particles, especially in the case of aragonite crystals. Different physical properties of produced filaments have been reflected in their mechanical performance.

In comparison with the reference sample, a decrease of tensile stress values has been measured, with one exception—filaments with synthetic aragonite. In this case, tensile stress was found to be higher for 12%. This behavior is explained by homogenous and unidirectional dispersion of aragonite's particles within the PP matrix and the ability of needle-like aragonite crystals to act as reinforced material, commonly used in the cement industry to improve mechanical performance. The produced $CaCO_3$ filaments may find their applications in 3D printing, and our next study will be focused on the characterization of printed products employing produced novel $CaCO_3$ filaments.

Author Contributions: Conceptualization, L.Z. and R.Š.; Methodology, L.Z. and R.Š.; Validation, J.P. and J.Š.; Formal analysis, L.Z., R.Š., D.M. and E.S.; Investigation, L.Z. and R.Š.; Resources, E.S.; Data curation, J.P.; Writing—original draft preparation, L.Z. and R.Š.; Writing—review and editing, J.P.; Visualization, D.M. and J.Š.; Supervision, L.Z.; Project administration, R.Š. All authors have read and agreed to the published version of the manuscript.

Funding: This research was funded by the Institute of Technology and Business under the project SVV 202108 and by the Czech Academy of Sciences, Institute of Theoretical and Applied Mechanics-RVO 68378297.

Institutional Review Board Statement: Not applicable.

Informed Consent Statement: Not applicable.

Data Availability Statement: Not applicable.

Conflicts of Interest: The authors declare no conflict of interest.

References

1. Lille, M.; Nurmela, A.; Nordlund, E.; Metsä-Kortelainen, S.; Sozer, N. Applicability of protein and fiber-rich food materials in extrusion-based 3D printing. *J. Food Eng.* **2018**, *220*, 20–27. [CrossRef]
2. Böckin, D.; Tillman, A.-M. Environmental assessment of additive manufacturing in the automotive industry. *J. Clean. Prod.* **2019**, *226*, 977–987. [CrossRef]

3. Serra, T.; Mateos-Timoneda, M.A.; Planell, J.A.; Navarro, M. 3D printed PLA-based scaffolds: A versatile tool in regenerative medicine. *Organogenesis* **2013**, *9*, 239–244. [CrossRef]
4. Zhakeyev, A.; Wang, P.; Zhang, L.; Shu, W.; Wang, H.; Xuan, J. Additive manufacturing: Unlocking the evolution of energy materials. *Adv. Sci.* **2017**, *4*, 1700187. [CrossRef]
5. Hambach, M.; Rutzen, M.; Volkmer, D. Properties of 3D-printed fiber-reinforced Portland cement paste. In *3D Concrete Printing Technology*; Elsevier: Amsterdam, The Netherlands, 2019; pp. 73–113.
6. Alexander, C. Streamlining automotive production with additive manufacturing. *Quality* **2018**, *57*, 37–39.
7. Rusling, J.F. Developing microfluidic sensing devices using 3D printing. *ACS Sens.* **2018**, *3*, 522–526. [CrossRef]
8. Culmone, C.; Smit, G.; Breedveld, P. Additive manufacturing of medical instruments: A state-of-the-art review. *Addit. Manuf.* **2019**, *27*, 461–473. [CrossRef]
9. Kessler, A.; Hickel, R.; Reymus, M. 3D printing in dentistry—State of the art. *Oper. Dent.* **2020**, *45*, 30–40. [CrossRef]
10. Zhang, J.; Jung, Y.-G. *Additive Manufacturing: Materials, Processes, Quantifications and Applications*; Butterworth-Heinemann: Oxford, UK, 2018; ISBN 0128123273.
11. Huang, W.D. How to treat additive manufacturing (3D printing) from a rational perspective. *Adv. Mater. Ind.* **2013**, *1*, 9–12.
12. Mwema, F.M.; Akinlabi, E.T. Basics of fused deposition modelling (FDM). In *Fused Deposition Modeling*; Springer: Cham, Switzerland, 2020; pp. 1–15.
13. Lyu, J.; Manoochehri, S. Online Convolutional Neural Network-based anomaly detection and quality control for Fused Filament Fabrication process. *Virtual Phys. Prototyp.* **2021**, *16*, 160–177. [CrossRef]
14. Yap, Y.L.; Sing, S.L.; Yeong, W.Y. A review of 3D printing processes and materials for soft robotics. *Rapid Prototyp. J.* **2020**, *26*, 1346–1361. [CrossRef]
15. Vanaei, H.R.; Shirinbayan, M.; Vanaei, S.; Fitoussi, J.; Khelladi, S.; Tcharkhtchi, A. Multi-scale damage analysis and fatigue behavior of PLA manufactured by fused deposition modeling (FDM). *Rapid Prototyp. J.* **2021**, *27*, 371–378. [CrossRef]
16. Kamaal, M.; Anas, M.; Rastogi, H.; Bhardwaj, N.; Rahaman, A. Effect of FDM process parameters on mechanical properties of 3D-printed carbon fibre–PLA composite. *Prog. Addit. Manuf.* **2021**, *6*, 63–69. [CrossRef]
17. Maurya, N.K.; Rastogi, V.; Singh, P. Fabrication of prototype connecting rod of PLA plastic material using FDM prototype technology. *Indian J. Eng. Mater. Sci.* **2021**, *27*, 333–343.
18. Scaffaro, R.; Maio, A.; Gulino, E.F.; Alaimo, G.; Morreale, M. Green Composites Based on PLA and Agricultural or Marine Waste Prepared by FDM. *Polymers* **2021**, *13*, 1361. [CrossRef]
19. Samykano, M. Mechanical Property and Prediction Model for FDM-3D Printed Polylactic Acid (PLA). *Arab. J. Sci. Eng.* **2021**, *46*, 7875–7892. [CrossRef]
20. Cress, A.K.; Huynh, J.; Anderson, E.H.; O'neill, R.; Schneider, Y.; Keleş, Ö. Effect of recycling on the mechanical behavior and structure of additively manufactured acrylonitrile butadiene styrene (ABS). *J. Clean. Prod.* **2021**, *279*, 123689. [CrossRef]
21. Venkatraman, R.; Raghuraman, S. Experimental analysis on density, micro-hardness, surface roughness and processing time of Acrylonitrile Butadiene Styrene (ABS) through Fused Deposition Modeling (FDM) using Box Behnken Design (BBD). *Mater. Today Commun.* **2021**, *27*, 102353.
22. Nathaphan, S.; Trutassanawin, W. Effects of process parameters on compressive property of FDM with ABS. *Rapid Prototyp. J.* **2021**, *27*, 905–917. [CrossRef]
23. Sardinha, M.; Vicente, C.M.S.; Frutuoso, N.; Leite, M.; Ribeiro, R.; Reis, L. Effect of the ironing process on ABS parts produced by FDM. *Mater. Des. Process. Commun.* **2021**, *3*, e151. [CrossRef]
24. Wang, B.; Chen, Y.; Qu, T.; Li, F. Structure and Properties of Multi-walled Carbon Nanotube/Acrylonitrile Butadiene Styrene Nanocomposite Specimens Prepared by Fused Deposition Modeling. *J. Macromol. Sci. B* **2021**, *60*, 77–87. [CrossRef]
25. Bakır, A.A.; Atik, R.; Özerinç, S. Effect of fused deposition modeling process parameters on the mechanical properties of recycled polyethylene terephthalate parts. *J. Appl. Polym. Sci.* **2021**, *138*, 49709. [CrossRef]
26. Özen, A.; Ganzosch, G.; Barchiesi, E.; Auhl, D.W.; Müller, W.H. Investigation of deformation behavior of PETG-FDM-printed metamaterials with pantographic substructures based on different slicing strategies. *Compos. Adv. Mater.* **2021**, *30*, 26349833211016476. [CrossRef]
27. Srinidhi, M.S.; Soundararajan, R.; Satishkumar, K.S.; Suresh, S. Enhancing the FDM infill pattern outcomes of mechanical behavior for as-built and annealed PETG and CFPETG composites parts. *Mater. Today Proc.* **2021**, *45*, 7208–7212. [CrossRef]
28. Panneerselvam, T.; Raghuraman, S.; Krishnan, N.V. Investigating Mechanical Properties of 3D-Printed Polyethylene Terephthalate Glycol Material Under Fused Deposition Modeling. *J. Inst. Eng. Ser. C* **2021**, *102*, 375–387. [CrossRef]
29. Carneiro, O.S.; Silva, A.F.; Gomes, R. Fused deposition modeling with polypropylene. *Mater. Des.* **2015**, *83*, 768–776. [CrossRef]
30. Wang, L.; Gardner, D.J. Effect of fused layer modeling (FLM) processing parameters on impact strength of cellular polypropylene. *Polymer* **2017**, *113*, 74–80. [CrossRef]
31. Elkins, K.; Nordby, H.; Janak, C.; Gray IV, R.W.; Helge Bohn, J.; Baird, D.G. Soft elastomers for fused deposition modeling. In Proceedings of the 1997 International Solid Freeform Fabrication Symposium, Austin, TX, USA, 11–13 August 1997.
32. Chaudhry, M.S.; Czekanski, A. Evaluating FDM process parameter sensitive mechanical performance of elastomers at various strain rates of loading. *Materials* **2020**, *13*, 3202. [CrossRef]
33. Ambrogi, V.; Carfagna, C.; Cerruti, P.; Marturano, V. Additives in Polymers. *Modif. Polym. Prop.* **2017**, 87–108. [CrossRef]
34. Crompton, T.R. *Chemical Analysis of Additives in Plastics*, 2nd ed.; Elsevier: Amsterdam, The Netherlands, 1977; ISBN 978-0-08-020497-0.

35. Bolgar, M.; Hubball, J.; Groeger, J.; Meronek, S. *Handbook for the Chemical Analysis of Plastic and Polymer Additives*, 2nd ed.; CRC Press: Boca Raton, FL, USA, 2015; ISBN 9781439860755.
36. Delva, L.; Hubo, S.; Cardon, L.; Ragaert, K. On the role of flame retardants in mechanical recycling of solid plastic waste. *Waste Manag.* **2018**, *82*, 198–206. [CrossRef]
37. Jonkers, N.; Krop, H.; van Ewijk, H.; Leonards, P.E.G. Life cycle assessment of flame retardants in an electronics application. *Int. J. Life Cycle Assess.* **2016**, *21*, 146–161. [CrossRef]
38. Al-Malaika, S.; Axtell, F.; Rothon, R.; Gilbert, M. Additives for Plastics. In *Brydson's Plastics Materials*; Elsevier: Amsterdam, The Netherlands, 2017; pp. 127–168.
39. Cherif Lahimer, M.; Ayed, N.; Horriche, J.; Belgaied, S. Characterization of plastic packaging additives: Food contact, stability and toxicity. *Arab. J. Chem.* **2017**, *10*, S1938–S1954. [CrossRef]
40. Rodriguez-Blanco, J.D.; Shaw, S.; Benning, L.G. The kinetics and mechanisms of amorphous calcium carbonate (ACC) crystallization to calcite, via vaterite. *Nanoscale* **2011**, *3*, 265–271. [CrossRef]
41. Ševčík, R.; Šašek, P.; Viani, A. Physical and nanomechanical properties of the synthetic anhydrous crystalline $CaCO_3$ polymorphs: Vaterite, aragonite and calcite. *J. Mater. Sci.* **2018**, *53*, 4022–4033. [CrossRef]
42. Nikolakakis, I.; Pilpel, N. Effects of particle size and particle shape on the tensile strengths of powders. *Powder Technol.* **1985**, *45*, 79–82. [CrossRef]
43. Gorna, K.; Hund, M.; Vučak, M.; Gröhn, F.; Wegner, G. Amorphous calcium carbonate in form of spherical nanosized particles and its application as fillers for polymers. *Mater. Sci. Eng. A* **2008**, *477*, 217–225. [CrossRef]
44. Adeosun, S.O.; Usman, M.A.; Akpan, E.I.; Dibie, W.I. *Characterization of LDPE Reinforced with Calcium Carbonate—Fly Ash Hybrid Filler*; University of Lagos: Lagos, Nigeria, 2014.
45. Rahman, G.M.S.; Aftab, H.; Islam, M.S.; Bin Mukhlish, M.Z.; Ali, F. Enhanced physico-mechanical properties of polyester resin film using $CaCO_3$ filler. *Fibers Polym.* **2016**, *17*, 59–65. [CrossRef]
46. Lin, H.; Dong, Y.; Jiang, L. Preparation of calcium carbonate particles coated with titanium dioxide. *Int. J. Miner. Metall. Mater.* **2009**, *16*, 592–597. [CrossRef]
47. Ihueze, C.C.; Mgbemena, C.O. Effects of reinforcement combinations of calcium carbonate nanofiller on the mechanical and creep properties of polypropylene. *J. Miner. Mater. Charact. Eng.* **2010**, *9*, 887. [CrossRef]
48. Rothon, R. *Particulate-Filled Polymer Composites*; iSmithers Rapra Publishing: Shrewsbury, UK, 2003; ISBN 1859573827.
49. Murphy, J. *Additives for Plastics Handbook*; Elsevier: Amsterdam, The Netherlands, 2001; ISBN 0080498612.
50. Wiebking, H. *Fillers in PVC, a Review of the Basics*; Specialty Minerals Inc.: Canaan, CT, USA, 1998; Volume 1.
51. Ševčík, R.; Mácová, P.; Estébanez, M.P.; Viani, A. Influence of additions of synthetic anhydrous calcium carbonate polymorphs on nanolime carbonation. *Constr. Build. Mater.* **2019**, *228*, 116802. [CrossRef]
52. Sarkar, A.; Mahapatra, S. Synthesis of all crystalline phases of anhydrous calcium carbonate. *Cryst. Growth Des.* **2010**, *10*, 2129–2135. [CrossRef]
53. *ČSN EN ISO 1133-1*; Plasty—Stanovení hmotnostního (MFR) a objemového (MVR) indexu toku taveniny termoplastů—Část 1: Standardní Metoda; Czech Agency for Standardization: Hradec Králové, Czech Rrepublic, 2012; Volume 28.
54. *ISO 25178*; Geometrical Product Specifications (GPS)—Surface Texture: Areal—Part 1: Indication of Surface Texture; ISO: Geneva, Switzerland, 2016.
55. *ISO 527-1:2019*; Plastics—Determination of Tensile Properties—Part 1: General Principles; ISO: Geneva, Switzerland, 2019.
56. Ševčík, R.; Pérez-Estébanez, M.; Viani, A.; Šašek, P.; Mácová, P. Characterization of vaterite synthesized at various temperatures and stirring velocities without use of additives. *Powder Technol.* **2015**, *284*, 265–271. [CrossRef]
57. Mann, S. Self-assembly and transformation of hybrid nano-objects and nanostructures under equilibrium and non-equilibrium conditions. *Nat. Mater.* **2009**, *8*, 781–792. [CrossRef]
58. Móczó, J. Particulate Filled Polymers, Interaction, Structure and Micromechanical Deformations. Ph.D. Thesis, Budapest University of Technology and Economics, Budapest, Hungary, 2004.
59. Cogswell, F.N. *Polymer Melt Rheology: A Guide for Industrial Practice*; Elsevier: Amsterdam, The Netherlands, 1981; ISBN 0857092987.
60. Aho, J. *Rheological Characterization of Polymer Melts in Shear and Extension: Measurement Reliability and Data for Practical Processing*; Tampere University of Technology: Tampere, Finland, 2011.
61. Lippmann, F. Crystal chemistry of sedimentary carbonate minerals. In *Sedimentary Carbonate Minerals*; Springer: Berlin/Heidelberg, Germany, 1973; pp. 5–96.
62. Leong, Y.W.; Ishak, Z.A.M.; Ariffin, A. Mechanical and thermal properties of talc and calcium carbonate filled polypropylene hybrid composites. *J. Appl. Polym. Sci.* **2004**, *91*, 3327–3336. [CrossRef]
63. Leong, Y.W.; Abu Bakar, M.B.; Ishak, Z.A.M.; Ariffin, A.; Pukanszky, B. Comparison of the mechanical properties and interfacial interactions between talc, kaolin, and calcium carbonate filled polypropylene composites. *J. Appl. Polym. Sci.* **2004**, *91*, 3315–3326. [CrossRef]
64. Da Costa, H.M.; Ramos, V.D.; Rocha, M.C.G. Rheological properties of polypropylene during multiple extrusion. *Polym. Test.* **2005**, *24*, 86–93. [CrossRef]
65. Rocha, M.C.G.; Silva, A.H.; Coutinho, F.M.B.; Silva, A.L.N. Study of composites based on polypropylene and calcium carbonate by experimental design. *Polym. Test.* **2005**, *24*, 1049–1053. [CrossRef]

66. Nikolakakis, I.; Pilpel, N. Effects of particle shape and size on the tensile strengths of powders. *Powder Technol.* **1988**, *56*, 95–103. [CrossRef]
67. Kalantari, B.; Huat, B.B.K. Peat soil stabilization, using ordinary portland cement, polypropylene fibers, and air curing technique. *Electron. J. Geotech. Eng.* **2008**, *13*, 1–13.
68. Małek, M.; Jackowski, M.; Łasica, W.; Kadela, M. Characteristics of recycled polypropylene fibers as an addition to concrete fabrication based on portland cement. *Materials* **2020**, *13*, 1827. [CrossRef]
69. Cioni, B.; Lazzeri, A. The role of interfacial interactions in the toughening of precipitated calcium carbonate–polypropylene nanocomposites. *Compos. Interfaces* **2010**, *17*, 533–549. [CrossRef]
70. Ansari, D.M.; Price, G.J. Correlation of the material properties of calcium carbonate filled polypropylene with the filler surface energies. *J. Appl. Polym. Sci.* **2003**, *88*, 1951–1955. [CrossRef]
71. Lyu, S.G.; Park, S.; Sur, G.S. The synthesis of vaterite and physical properties of PP/CaCO 3 composites. *Korean J. Chem. Eng.* **1999**, *16*, 538–542. [CrossRef]
72. Lin, Y.; Chen, H.; Chan, C.-M.; Wu, J. Effects of coating amount and particle concentration on the impact toughness of polypropylene/CaCO3 nanocomposites. *Eur. Polym. J.* **2011**, *47*, 294–304. [CrossRef]
73. Yang, K.; Yang, Q.; Li, G.; Zhang, Y.; Zhang, P. Mechanical properties and morphologies of polypropylene/single-filler or hybrid-filler calcium carbonate composites. *Polym. Eng. Sci.* **2007**, *47*, 95–102. [CrossRef]
74. He, E.; Shang, W.; Chen, S. Proceedings of the IEEE International Conference on Properties and Applications of Dielectric Materials, Xi'an, China, 21–26 June 2000; Volume 1, p. 431.